Core-Level Spectroscopy of Point Defects in Single Layer *h*-BN

Kazu Suenaga,* Haruka Kobayashi, and Masanori Koshino

Nanotube Research Center, National Institute of Advanced Industrial Science and Technology (AIST),
Central 5, Tsukuba 305-8565, Japan

(Received 23 November 2011; published 13 February 2012)

Electron energy-loss spectroscopy (EELS) is used to analyze single-layered hexagonal boron-nitride with or without point defects. EELS profiles using a 0.1 nm probe clearly discriminate the chemical species of single atoms but show different delocalization of the boron and nitrogen K edges. A monovacancy at the boron site is unambiguously identified and the electronic state of its nearest neighboring nitrogen atoms is examined by energy-loss near edge fine structure analysis, which demonstrates a prominent defect state. Theoretical calculations suggest that the observed prepeak originates from the 1s to lowest unoccupied molecular orbital excitation of dangling nitrogen bonds, which is substantially lowered in energy with respect to the three coordinated nitrogen atoms.

DOI: 10.1103/PhysRevLett.108.075501 PACS numbers: 61.72.−y, 61.48.De, 68.37.Ma, 81.05.ue

Structural defects often govern the properties of materials. In low-dimensional materials, especially the interrupted periodicities (atomic defects or edge structures) are quite important since they strongly affect their physical properties. In bulk crystals electron microscopes have been widely used to examine structural defects such as dislocations and stacking faults (or grain boundaries), which are regarded as one- and two-dimensional structural defects, respectively. In contrast, investigating individual point defects (zero-dimensional defects, such as monovacancies) was believed to be difficult because this requires both atomic sensitivity and atomic resolution. Also, specimens need to be very thin such that one can detect the individual point defects from image contrast in transmission electron microscopy (TEM).

After a monovacancy was first observed by TEM and proved to be stable even in low-dimensional carbon structures [1], studies of point defects in monolayered materials have become very popular among scientists. Vacancies and topological defects in graphene are commonly examined at atomic level [2–4]. Defects and edge structures in hexagonal boron nitride (*h*-BN) are also a hot topic among physicists [5–7]. Recently, monovacancies have been successfully identified in WS_2 nanoribbons [8]. Krivanek *et al.* have shown that the atomic species in *h*-BN can be simply identified by annular dark field (ADF) signal intensities [9], however their analysis still lacks direct evidence for the elemental assignment. Electron energy-loss spectroscopy (EELS), which measures a projection of the joint density of states, is more appropriate to assign the chemical species with atomic resolution.

Here we describe a spatially resolved EELS study of an *h*-BN single layer with and without atomic defects to identify the atomic structures with elemental assignment. The inevitable delocalization of EELS signals is suggested to practically limit the achievement of using EELS for chemical mapping with atomic resolution. The boron monovacancy (V_B) is assigned as a typical point defect by ADF imaging and EELS, and energy-loss near edge fine structure (ELNES) is used to investigate the electronic states of nitrogen atoms around the point defect. The work provides an example of spectroscopic imaging based on the scanning transmission electron microscopy (STEM)-EELS techniques to demonstrate the possibilities of exploring the electronic states with single atom sensitivity.

A JEM-2100F equipped with a delta corrector and cold field emission gun was operated at 60 kV in these experiments [10,11]. Commercially available *h*-BN powder was cleaved and transferred to microscopy Au grids [12]. As seen in Fig. 1(a), *h*-BN flakes can be peeled off layer-by-layer during the STEM observation [5] and small regions finally become single-layer domains (indicated by arrows). A fast Frourier transform (FFT) of the typical ADF image shows that the microscope can resolve 0.108 nm in the STEM mode (not shown). The probe current was ~40 pA.

Figure 1(b) shows an ADF image of single-layered *h*-BN that is free from structural defect. Figure 1(c) is a corresponding atomic model where a line-spectrum has been recorded (indicated by a yellow line from A to B). A series of 50 spectra have been recorded with a step size of ~0.02 nm (Fig. S1) [13]. Each spectrum is acquired in 0.2 sec. Since the specimen is very fragile and is easily damaged during the observation, the experiment must be done with the minimum dose of electron beam. The counting efficiency is therefore optimized at the cost of energy resolution (~ 1 eV realized by binning 4 channels). A typical EELS spectrum (a sum of four) is shown and reflects the normal sp^2 bonded *h*-BN structure, involving the sharp π^* and σ^* for both B and N K edges commonly observed [14]. The intensities of the K edges are integrated after the background extraction (Fig. S1b).

Figure 2 shows the intensity profiles of the ADF, boron K-edge and nitrogen K-edge signals. Four local maxima in

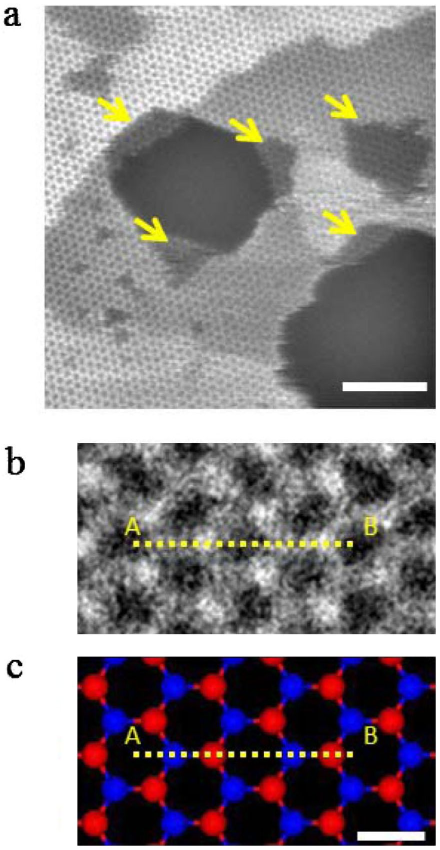

FIG. 1 (color online). (a) ADF image of layer-by-layer peeled flake of *h*-BN. Single-layered regions are indicated by yellow arrows. Scale bar = 2 nm. (b),(c) ADF image of single-layered *h*-BN without defects and its modeled structure (red: nitrogen, blue: boron). Scale bar = 0.2 nm (white solid line). The zero level of the image has been adjusted to improve the image contrast.

the ADF profile correspond to the two boron and two nitrogen atoms. Because the ADF signals monotonically increase with atomic number (Z), the higher maxima in the ADF profile corresponds to the nitrogen atomic positions ($Z = 7$) and the lower maxima to the boron ($Z = 5$) [9]. This is confirmed by the nitrogen K-edge profile which shows two maxima indeed coinciding with the higher maxima in ADF profile. However, one can easily notice that the nitrogen K-edge intensity does not go down to zero even between two nitrogen atoms. This is a clear proof that the nitrogen profile is affected by the EELS signal delocalization [15]. The large probe tail and mechanical instabilities such as the specimen drift during the line scan may also contribute partly to the nonzero intensity but this should not be a dominant effect because the simultaneously recorded ADF profile clearly shows well-separated atoms. Note that there should be no channeling effect because the specimen is only one-atom thick.

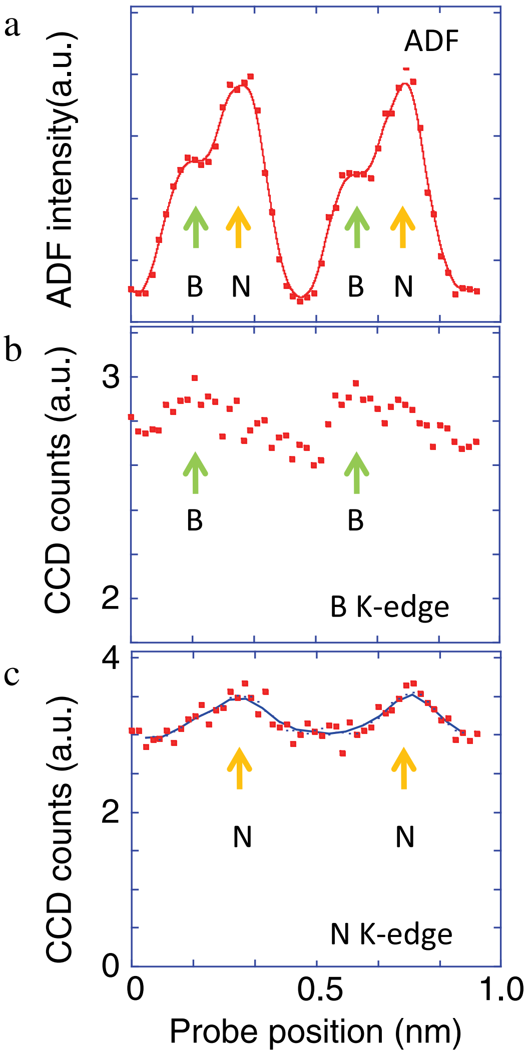

FIG. 2 (color online). (a),(b),(c) Profiles for intensities of ADF, boron K-edge and nitrogen K-edge recorded along the yellow line in Fig. 1. The ADF profile clearly reveals the B and N atomic positions. The nitrogen K-edge intensity shows the local maxima coincides to the N atomic positions while the boron K edge shows a similar local maxima but much flat distribution due to the possible EELS signal delocalization. Principal component analysis (PCA) was performed to extract the boron K-edge profile.

More interesting is the profile of the boron K edge. The boron profile shows similar maxima at the boron atomic positions in the ADF profile, but these maxima are less visible in comparison with the nitrogen profile. The boron K edge shows only a few percent difference in its intensity when the probe is on and off the boron atoms, while it is around 25% for the nitrogen K edge. This different behavior in the profiles of the boron and nitrogen K edges can be attributed to the energy-loss dependence of EELS signal delocalization. In a simple classical theory, the degree of EELS delocalization is most simply expressed by

$$b = hv/\Delta E,$$

where b is the impact parameter, v is the speed of incident electron, h is the Plank constant and ΔE is the energy loss [16]. This simple equation implies that the delocalization is larger at the boron K edge (~ 200 eV) than at the nitrogen

K-edge (~ 400 eV) by a factor of 2. They are indeed estimated as 0.15 and 0.08 nm for the boron and nitrogen *K* edges, respectively. It is therefore more difficult to see the local maxima in the boron *K*-edge profile rather than in the nitrogen case. Despite the inevitable delocalization effect, we are still able to discriminate between constituent atoms in the *h*-BN single layer, which is very crucial to identify the point defect structures.

Figure 3 shows a set of spatially resolved EELS analysis of a single-layered *h*-BN with a point defect. As shown in Fig. 3(a), a monovacancy is induced at the boron site by the knock-on effect, which can be proved by the fact that the darkest contrast appears in the middle of three nitrogen atoms showing brighter contrast. Such a boron monovacancy (V_B) has also been seen previously [5,6]. A line spectrum is recorded across the V_B along the yellow arrow shown in Fig. 3(b). The experimental condition for EELS acquisition is the same as above. From the line-spectrum three typical spectra for the nitrogen *K* edge have been extracted, the probe positions of those approximately correspond to the yellow circles in Fig. 3(c). Note that the size of the yellow circles roughly reflects the region where the EELS signal comes from, which actually include the probe diameter of our instrument [17] and the estimated delocalization effect. While the first and third spectra are quite similar to the one for the sp^2 bonded nitrogen atoms in *h*-BN with the known π^* peak at 401 eV, the second spectrum recorded near the V_B indeed shows a sharp prepeak around 392 eV. Although the spectra are rather noisy due to the minimized acquisition time, this prepeak appears at the same energy-level in many different experiments and reproducibly arises at the other V_B sites (see also Fig. S2) [13]. The prepeak has never been observed so far to the best of our knowledge and should reflect the peculiar electronic state around the V_B. Note that three nitrogen atoms around the vicinity of the V_B can be contributing to the second spectrum.

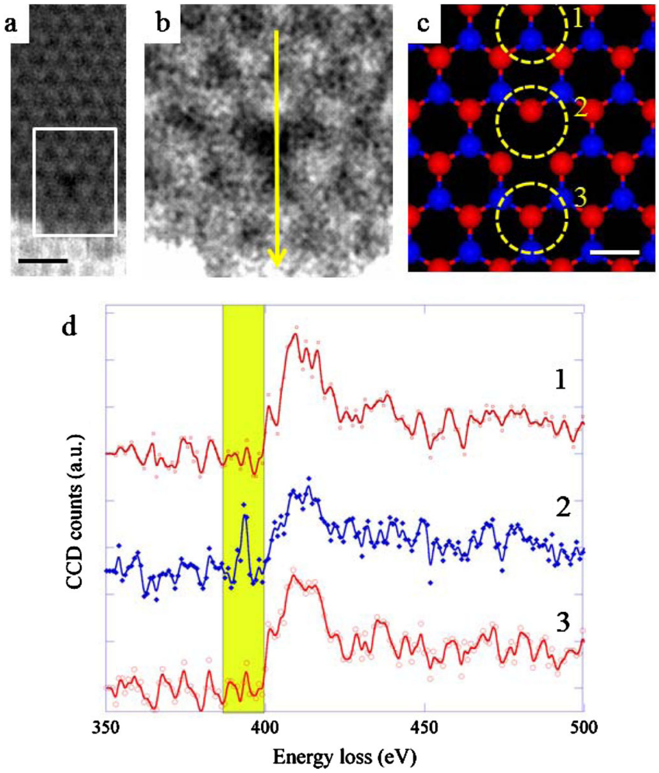

FIG. 3 (color online). (a) ADF image shows a monovacancy in a single layer *h*-BN. Scale bar = 0.3 nm. (b),(c) Close up view of the rectangle in (a) shows the boron monovacancy (V_B) and its schematic presentation (red: nitrogen, blue: boron). Scale bar = 0.2 nm. Line-spectrum was recorded across the yellow arrow in (b). (d) Nitrogen *K*-edge fine structures extracted from the line spectrum. Each of three approximately corresponds to the probe positions marked in (c). A prominent prepeak in the nitrogen *K* edge can be found at 392 eV (highlighted in yellow) in the spectrum recorded at the position 2, i.e., near the boron vacancy site.

There is no nitrogen monovacancy (V_N) found in our experimental condition. The kinetic condition when the boron and nitrogen atoms are knocked-on by fast electrons has been well discussed in previous literature [18]. In addition to the formation energy difference between V_B and V_N, the chemical etching effect due to the residual gas in the microscope chamber should be considered for the selective sputtering effect of boron atoms.

In order to corroborate this defect-specific fine structure of the nitrogen *K* edge, two different theoretical calculations can be performed. One is the molecular orbital (MO) calculation with a discrete variance $X\alpha$ method (DV-$X\alpha$) based on a small cluster structure (Fig. S3a–c, g–j) and the other is the band calculation using a periodic structure (WIEN2K, see Fig. S3d–f). Here, we show only the result of the MO calculation. The other data are shown in the supplemental materials [13].

We first constructed a molecule of $B_{19}N_{18}$ as one of the smallest sized clusters in which nitrogen atoms near the center were not significantly influenced by the conditions of peripheral atoms. Termination of peripheral atoms with hydrogen substantially stabilized the whole system. Thus $B_{18}N_{18}H_{15}^-$ and $B_{19}N_{18}H_{15}$ molecules were geometrically optimized by using the PWC functionals [19], which represent the *h*-BN with and without the V_B. The EELS fine structures were then simulated as the partial density of states of unoccupied $2p$ orbitals (see also the result of the transition probability in Fig. S3a–c). The core-hole effect was considered by using the transition-state approximation [20], which roughly gives us the threshold energy of the nitrogen *K* edge by introducing a half electron removed from the nitrogen $1s$ orbital and then added to an unoccupied orbital [21]. A -1 charge was equally divided among three nitrogen atoms neighboring V_B.

Results of the calculations are shown in Fig. 4. The ELNES simulation for the nitrogen *K* edge well reproduces the experimental data when there is no boron vacancy [Fig. 4(a)]. There is a noticeable difference in the threshold energy because the π^* peak arises at 398.6 eV in the

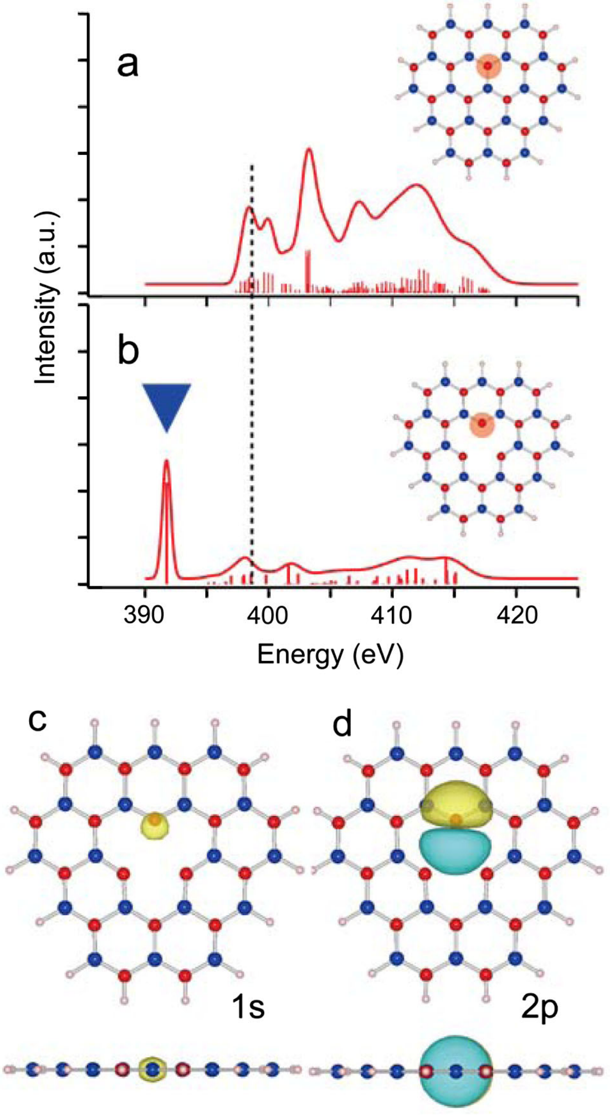

FIG. 4 (color online). ELNES simulation of nitrogen K edge for a single-layered h-BN. (a) ELNES (partial DOS of unoccupied $2p$ orbitals) of a nitrogen atom marked by a red circle in which a core-hole was introduced shows π^* peak around 398.6 eV. (b) With a V_B defect, the neighboring nitrogen atom exhibits a sharp π^* peak at 391.7 eV (marked by a blue arrowhead and −6.9 eV shifted). The LUMO state of nitrogen atom next to the V_B largely contributes to the shifted π^* peak. (c), (d) Contour map of $1s$ and $2p$ orbitals shows a distribution of the wave function from the nitrogen atom towards V_B (vertical view on top and horizontal view on bottom relative to h-BN plane). Thus the defect-related state (an arrowhead in b) can be more localized towards the V_B site. Yellow and blue colors represent positive and negative component of wave functions. The level of the isosurface is set to $0.01\ \mathrm{a}_0^{-3}$, where a_0 represents the Bohr radius.

simulation while at 401.0 eV in experiment. By introducing the V_B, the threshold energy is significantly shifted to lower energy and dominantly contributes to a sharp π^* peak appearing at 391.7 eV [an arrowhead in Fig. 4(b)]. Contour maps show the spatial distribution of the wave function of the $1s$ state [Fig. 4(c)] at core-energy and the $2p$ state at the lowest unoccupied molecular orbital (LUMO) [Fig. 4(d)] from one of the nitrogen atoms at the vicinity of the V_B. In Fig. 4(c), the $1s$ orbital is asymmetric and extends in the direction of the V_B which is different from the spherical $1s$ orbital of nitrogen without V_B (see Fig. S3g). The nitrogen $2p$ orbital in Fig. 4(d) is one of the major components of the LUMO as seen from Fig. S3i. The node of the nitrogen $2p$ orbital at the LUMO state is located near the V_B defect and there are three equivalent nitrogen atoms adjacent to the V_B. The excitation from $1s$ to LUMO [an arrowhead in Fig. 4(b)] could thus be enhanced near the V_B.

In this experiment, we clearly show the atom-by-atom analysis of single-layer h-BN by means of spatially resolved EELS. This is a great step further beyond the previous report showing the chemical analysis of h-BN by the simple ADF intensities or phase contrast [9,22]. Also the electronic state of single vacancies is successfully demonstrated by EELS fine structure analysis and by theoretical calculations.

This work is partially supported by the JST-CREST program. K. S. and M. K. acknowledge support of the Grant-in-Aid for Scientific Research from MEXT (19054017 and 23681026).

---

*suenaga-kazu@aist.go.jp

[1] A. Hashimoto *et al.*, Nature (London) **430**, 870 (2004).
[2] K. Suenaga *et al.*, Nature Nanotech. **2**, 358 (2007).
[3] J. Meyer *et al.*, Nano Lett. **8**, 3582 (2008).
[4] C. O. Girit *et al.*, Science **323**, 1705 (2009).
[5] C. Jin *et al.*, Phys. Rev. Lett. **102**, 195505 (2009).
[6] J. Meyer *et al.*, Nano Lett. **9**, 2683 (2009).
[7] N. Alem *et al.*, Phys. Rev. B **80**, 155425 (2009).
[8] Z. Liu *et al.*, Nature Commun., **2**, 213 (2011).
[9] O. Krivanek *et al.*, Nature (London) **464**, 571 (2010).
[10] T. Sasaki *et al.*, J. Electron Microsc. **59**, S7 (2010).
[11] K. Suenaga and M. Koshino, Nature (London) **468**, 1088 (2010).
[12] D. Pacile, J. C. Meyer, C. O. Girit, and A. Zettl, Appl. Phys. Lett. **92**, 133107 (2008).
[13] See Supplemental Material at http://link.aps.org/supplemental/10.1103/PhysRevLett.108.075501 for additional data.
[14] K. Suenaga *et al.*, Appl. Phys. A **68**, 301 (1999).
[15] D. A. Muller and J. Silcox, Ultramicroscopy **59**, 195 (1995).
[16] K. Suenaga, Y. Iizumi, and T. Okazki, Eur. Phys. J. Appl. Phys. **54**, 33 508 (2011).
[17] The d_{59} probe diameter where 59% of total current is involved can be estimated as 130 pm. See K. Sasaki *et al.*, Micron (2011).
[18] J. Kostakosiki *et al.*, Phys. Rev. B **82**, 113404 (2010).
[19] J. P. Perdew and Y. Wang, Phys. Rev. B **45**, 13244 (1992).
[20] T. Mizoguchi *et al.*, Phys. Rev. B **61**, 2180 (2000).
[21] J. C. Slater and K. H. Johnson, Phys. Rev. B **5**, 844 (1972).
[22] J. Meyer *et al.*, Nature Mater. **10**, 209 (2011).